Eur. Phys. J. D **28**, 323–330 (2004)
DOI: 10.1140/epjd/e2003-00325-0

THE EUROPEAN PHYSICAL JOURNAL D

Two-step laser optogalvanic spectroscopy of the odd-parity Rydberg states of atomic mercury

M.A. Zia[1,2] and M.A. Baig[1,a]

[1] Atomic and Molecular Physics Laboratory, Quaid-i-Azam University, Islamabad, Pakistan
[2] Optics Laboratory, P.O. Box 1021, Islamabad, Pakistan

Received 11 September 2003 / Received in final form 5 November 2003
Published online 20 January 2004 –

Abstract. We present new experimental data on the highly excited levels in mercury using the two-step laser excitation and optogalvanic detection technique in conjunction with a RF discharge cell. The $6s7s\ ^3S_1$ intermediate level has been accessed from the $6s6p\ ^3P_2$ metastable level that is collisionally populated in the mercury discharge in the presence of a buffer gas at a pressure of about 1 Torr. Two beams from two different dye lasers pumped with a common excimer laser were passed through the discharge cell containing mercury vapors. The first laser was tuned to $6s7s\ ^3S_1$ level whereas the second laser was scanned covering the wavelength region between 544–458 nm. We have observed the $6snp\ ^3P_0$ ($10 \leq n \leq 18$), $6snp\ ^3P_1$ ($10 \leq n \leq 41$), $6snp\ ^3P_2$ ($10 \leq n \leq 70$) and $6snp\ ^1P_1$($10 \leq n \leq 42$) Rydberg series. The $6snp\ ^3P_2$ Rydberg series to such high n-value has been reported for the first time. The first ionization potential of mercury is determined from the $6snp\ ^3P_2$ Rydberg series as 84184.15±0.05 cm^{-1}. Some collisionally induced parity forbidden transitions have also been located that are identified as $6sns\ ^1S_0$ ($40 \leq n \leq 58$) series.

PACS. 31.50.-x Potential energy surfaces – 32.30.Jc Visible and ultraviolet spectra – 32.80.Rm Multiphoton ionization and excitation to highly excited states (e.g., Rydberg states)

1 Introduction

Laser optogalvanic spectroscopy is a sensitive and simple technique to probe the spectral characteristics of atoms and molecules generated in a discharge. Laser optogalvanic signals arise due to the change in the impedance of the discharge in response to the laser radiation propagating through a discharge tube and this variation is monitored as a change in the voltage across the electrodes in the discharge cell. As the laser wavelength matches a dipole allowed transition in the active medium, absorption takes place and as a result impedance of the discharge alters. Therefore, laser excited optogalvanic spectra are similar to that recorded in emission or absorption accessed from different atomic levels. The DC discharge cells have been extensively used in the detection of high Rydberg states in atoms and molecules as well as it provides sharp lines that serve as wavelength standards in the dye laser based experiments [1–5]. Much of the work on the low-lying levels in mercury has been performed using low-pressure and high-pressure DC discharge [6,8]. Wan de Weijer and Cramers [7] determined the lifetime of $6s6p\ ^3P_1$ atomic levels of mercury in a low pressure discharge by exciting the $6s6p\ ^3P_0$ to $6s7s\ ^3S_1$ level and studied the time dependence of the radiative decay of $6s6p\ ^3P$ levels. Subsequently, Kramer [8] investigated the above mentioned transitions in a high-pressure mercury discharge. Richardson et al. [9] presented a detailed experimental and theoretical study of the optogalvanic effect induced in a Hg–Ar discharge at 546.1 nm laser wavelength. Benck et al. [10] reported the lifetimes, branching ratios and absolute transition probabilities for a number of levels in mercury using time resolved laser induced fluorescence technique. Doppler free spectroscopy has been used to study the isotopic shifts and hyperfine splitting by Sarger et al. [11]. The energy transfer in mercury vapor following laser excitation of the $6s7s\ ^1S_0$ state via two photon absorption has been investigated by Bras et al. [12]. The $6snp\ ^1P_1$ and $^3P_1$ Rydberg series were reported by Baig [13]. using synchrotron radiation and the first ionization potential of mercury was also determined. The $6snp\ ^1P_1$ and $^3P_1$ Rydberg series are perturbed around $n = 9$ by the leading member of the $5d(^2D_{5/2})np$ series ($n = 6$). Consequently, the multichannel quantum defect theory was used to extract the information pertaining to series perturbations and the ionization potential of mercury.

Tursunov et al. [14] reported the $6snp\ ^3P_{0,1,2}$ Rydberg series using three-step laser excitation from the ground state and extended the series up to $n = 60$. Recently, Kasimov et al. [15] reported the $6snp\ ^1P_1$ Rydberg series

[a] e-mail: baig@qau.edu.pk

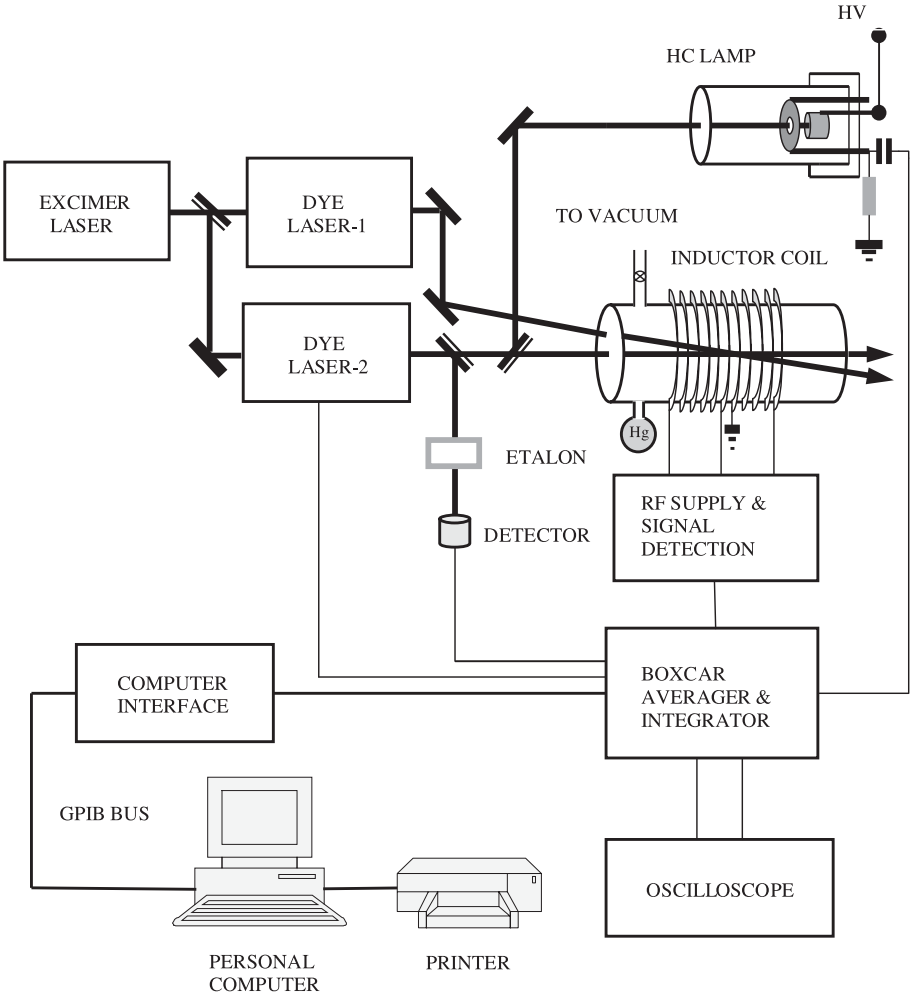

Fig. 1. Schematic diagram of the experimental to record the two-step excitation spectra of mercury.

in the range of $n = 15$ to 50 by using the $6s7s\ ^1S_0$ as an intermediate level. They also presented the shape of the $5d^9 6s^2 6p\ ^1P_1$ autoionizing resonance adjacent to the first ionization limit. The excitation cross-section of this resonance at 402.0 nm was also reported as $\sigma = 2.8 \times 10^{-15}$ cm^2 by employing the saturation technique.

Using a four-photon resonant ionization of mercury, Tai and Dalby [16] observed the $6snp\ ^{1,3}P_1$ ($8 \leq n \leq 14$) and $6snf\ ^1F_3$ ($5 \leq n \leq 11$) series. The present work was motivated to extend the odd parity $6snp\ ^{1,3}P_{0,1,2}$ Rydberg series close to the ionization limit. In the present experiment, we have used two-step laser excitation and optogalvanic detection in conjunction with RF discharge to observe the $6snp\ ^3P_{0,1,2}$ and $6snp\ ^1P_1$ Rydberg states in mercury from the $6s7s\ ^3S_1$ intermediate level. As a result, the $6snp\ ^3P_2$ series has been extended up to $n = 70$, a substantial improvement in the existing data. Consequently, an improved value of the first ionization of mercury has been determined. The present value of the ionization potential is in excellent agreement to that reported by Baig et al. [17] who used high resolution photoabsorption detection in conjunction with synchrotron radiation background source.

2 Experimental set-up

A schematic diagram of the apparatus used in this experiment is shown in Figure 1. A locally designed and developed radio frequency source at 4.0 M Hz has been used to excite the discharge. The inductor coil in the RF source was 40 mm long, 32 mm in diameter having 24 turns. The rating of the power supply was 50 V and 500 mA. A Pyrex cell 100 mm long, 30 mm diameter and a small bulb, to contain mercury along with Pyrex windows, was used to create the RF discharge. The cell was evacuated up to 10^{-6} Torr and subsequently neon gas was filled as a buffer gas at 1 to 2 Torr pressure. A steady discharge in the cell was sustained with RF source by applying initially a high amplitude pulse. The optogalvanic signal was detected through the same inductor coil used to run the RF discharge [18].

An excimer pumped dye laser (Lambda Physik) system has been used in this experiment. Two dye lasers were pumped with a common excimer laser, one was commercial (Lambda Physik FL 2002-EC) and the other was a locally developed that was pumped by 10% beam of the excimer laser. This dye laser was fixed at

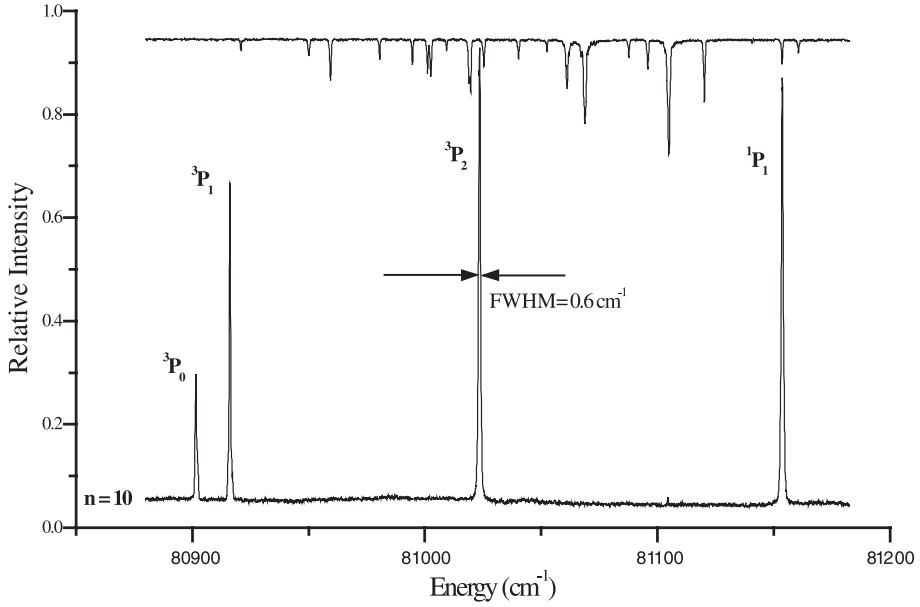

Fig. 2. The spectrum of mercury in the energy region 80880 to 81180 cm^{-1} that corresponds to $n = 10$, showing the relative intensities of the four lines: $^3P_{0,1,2}$ and $^1P_1$. The top spectrum is the optogalvanic of neon hollow cathode lamp.

546.07 nm that promoted the mercury atoms from the $6s6p\ ^3P_2$ metastable level to the $6s7s\ ^3S_1$ level. The second dye laser charged with Coumarin 540-A, Coumarin 500, Coumarin 102 and Coumarin 47 dissolved in methanol was scanned to cover the region from 544.0 nm to 458.0 nm.

For the wavelength calibration and determination of the energies of the unknown mercury lines, the main dye laser beam was split in to three parts. The major portion of the dye laser beam was directed through the RF discharge cell to register the Rydberg states of mercury. About 10% of the beam was directed into a neon filled hollow cathode lamp and about 10% in to a 5.1 mm thick Fabry-Perot etalon, FSR 0.67 cm^{-1} and finesse 16 (Lambda Physik FL-82). The optogalvanic effect in the neon filled hollow cathode lamp produces well distributed neon spectra, accurately known and listed in the MIT table [19], that are used for calibration. The interference fringes from the etalon serve as the relative frequency scale of the dye laser. The three signals were simultaneously recorded using three Box Car Averagers (SR250) and the data were stored on a PC through a GPIB BUS for subsequent analysis. There are about forty data points between the two consecutive etalon rings. Thus, through the calibration process the energies at the peak positions have been measured with an accuracy better than ± 0.05 cm^{-1}.

3 Results and discussion

There are four Rydberg series converging to the first ionization limit, which can be reached by two-step excitation from the $6s6p\ ^3P_2$ metastable state of mercury via the $6s7s\ ^3S_1$ intermediate level. The $6s6p\ ^3P_2$ metastable state gets populated due to the RF discharge in the cell containing mercury vapors. When mercury atoms are transferred from the $6s6p\ ^3P_2$ to the $6s7s\ ^3S_1$ level using 546.07 nm laser, the $6s7s\ ^3S_1$ level decays to the $6s6p\ ^3P$ multiplets. The lifetime of the $6s7s\ ^3S_1$ level is 8.0(4) ns and its population redistribution to the $6s6p\ ^3P_2$, $^3P_1$ and $^3P_0$ levels is 38.8%, 44.6% and 16.6% respectively [10]. The transition probabilities from $6s7s\ ^3S_1$ to $6s6p\ ^3P_2$, $6s6p\ ^3P_1$ and $6s6p\ ^3P_0$ are $1.46(11) \times 10^8$ s^{-1}, $1.67(13) \times 10^8$ s^{-1} and $0.62(6) \times 10^8$ s^{-1} respectively [20]. Since the lifetime of $6s7s\ ^3S_1$ is 8.0 ns and the dye laser pulse width is 10 ns therefore, the temporal overlap of the two dye lasers was not so critical. The second laser excites the atoms from $6s7s\ ^3S_1$ to the $6snp\ ^3P_{0,1,2}$ and $^1P_1$ Rydberg levels. In the strict LS-coupling schemes, transitions from ^3S to ^3P are favored whereas, singlet transitions are forbidden according to $\Delta S = 0$ selection rule. However, the observed structure shows $^3P_{0,1,2}$ and $^1P_1$ lines of comparable intensity, which is an indication of a departure from the LS-coupling to a more appropriate representation of jj-coupling for the level designation. The four Rydberg series designated in LS- and jj-coupling schemes are:

$$\begin{aligned} 6s7s\ ^3S_1 \rightarrow 6snp\ ^3P_0 \quad & (1/2,1/2)_0 \\ 6snp\ ^3P_1 \quad & (1/2,1/2)_1 \\ 6snp\ ^3P_2 \quad & (1/2,3/2)_2 \\ 6snp\ ^1P_1 \quad & (1/2,3/2)_1. \end{aligned}$$

We have observed the $6snp\ ^3P_0$ series up to $n = 18$, $6snp\ ^3P_1$ series up to $n = 41$ and $6snp\ ^3P_2$ series up to $n = 70$ whereas, the $6snp\ ^1P_1$ series has been observed up to $n = 42$.

Figure 2 shows the optogalvanic spectrum of mercury recorded in the energy region 80880 to 81182 cm^{-1}. The upper trace shows the optogalvanic spectrum of neon filled hollow cathode lamp that serves as wavelength standards to determine the energies of the mercury lines. Four peaks are evident which are identified as $6s10p\ ^3P_{0,1,2}$ and $^1P_1$ respectively in the order of increasing energy. As far as the relative intensities of the lines are concerned, the $^3P_0$ line is the weakest whereas, $^3P_2$ and $^1P_1$ posses nearly

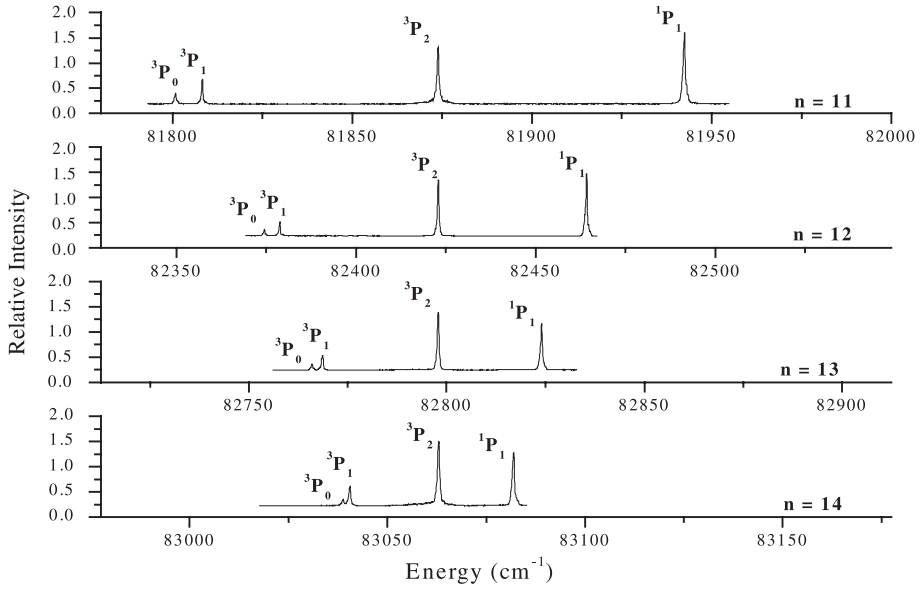

Fig. 3. The multiplets structure of mercury for $n = 11$ to $n = 14$, that shows the trend of the relative intensities of the four multiplets and the merging of the $^3P_0$ line with the $^3P_1$ line.

the same intensity that is about three times higher than the $^3P_0$ line. It is also noted that the widths of the spectra lines, FWHM are $\cong$0.6(2) cm^{-1} that remain constant as the principal quantum number increases. The line width, as shown for the $6s10p\ ^3P_2$ line in Figure 2, is much larger than the laser band width $\cong$0.2 cm^{-1}. The enhanced width may be attributed to the Doppler broadening and power broadening. The contribution of the Doppler broadening is estimated as 0.02 cm^{-1} using the relation:

$$\delta\upsilon_d = \upsilon_0 7.16 \times 10^{-7} \times \sqrt{T/M},\ T = 70\ ^\circ\mathrm{C} \text{ and } M = 200.$$

The lifetime of the $6s7s\ ^3S_1$ intermediate level is 8 ns and its contribution in the widths of the observed lines is also negligible. One additional contribution to the line broadening may be due to the mercury isotopes. The energy spread of the five abundant isotopes in mercury is about 0.7 cm^{-1} [21]. However, in the present experiment we are unable to observe the isotopic shifts.

We have also noticed a sharp deviation from the Lande's interval rule in the triplet spectra of mercury. The ratio of the energy interval among the $^3P_2$–$^3P_1$ and $^3P_1$–$^3P_0$ lines is 7.41 at $n = 10$ and it enhances from 14.51 to 46.17 at $n = 14$ and 18 respectively. Whereas, for the $6s6p\ ^3P$ lines listed in the NBS tables [22], this ratio is 2.62 instead of 2.0 according to the Lande's interval rule. The drastic deviation from the Lande interval rule can be ascribed to the singlet-triplet mixing or mixing of other states. The observed lines in the sp-configuration, in terms of Slater integrals, are represented by the relations [23]:

$$E\ (^1P_1) = F_0 - \xi_p/4 + \sqrt{(G_1 + \xi_p/4)^2 + \xi_p^2/2}$$
$$E\ (^3P_2) = F_0 - G_1 + \xi_p/2$$
$$E\ (^3P_1) = F_0 - \xi_p/4 - \sqrt{(G_1 + \xi_p/4)^2 + \xi_p^2/2}$$
$$E\ (^3P_0) = F_0 - G_1 - \xi_p$$

where F_0 is just an additive constant representing the coulomb part, G_1 is the measure of the exchange integral and ξ_p is the spin-orbit interaction parameter. The values of the Slater Integrals can be extracted from the observed transition energies using the following relations:

$$F_0 = \left[^1P_1 + {}^3P_1\right]/2 + \left[^3P_2 - {}^3P_0\right]/6$$
$$G_1 = \left[(^1P_1 + {}^3P_1) - (^3P_2 + {}^3P_0)\right]/2$$
$$\xi_p = 2\left[(^3P_2 - {}^3P_0)\right]/3.$$

The values of G_1 (cm^{-1}) are 5896.5, 72.6, 7.34 and 3.20 whereas, the values of ξ_p (cm^{-1}) are 4265.3, 80.4, 11.89 and 5.67 for $n = 6$, 10, 15 and 18 respectively. The corresponding ratios of the electrostatic to that of the spin-orbit interaction for the n values are 1.38, 0.90, 0.62 and 0.56 respectively. An additional information about a more appropriate coupling scheme for level designation can be extracted from the coupling parameter "Φ" which is defined as [24]:

$$\Phi = \frac{^3P_2 - {}^3P_0}{^1P_1 + {}^3P_1 - 2\ {}^3P_0}.$$

The value of the coupling parameter varies from zero to one for the LS- and jj-coupling schemes. The calculated coupling parameter is 0.352, 0.454, 0.548 and 0.57 for $n = 6$, 10, 15 and 18 respectively. This exercise clearly reflects that at lower n-values the levels can well be described in the LS-coupling. Around $n = 10$, the spin-orbit and electrostatic parameters are nearly equal and the coupling parameter "Φ" is 0.454, thus intermediate coupling will be more appropriate. After $n = 18$ the spin-orbit interaction parameter becomes nearly double that of the electrostatic interaction parameter. Therefore, the best coupling scheme for mercury will be either JK or jj as has been perceived in the analysis of the $4d$-subshell excitation spectrum of mercury [25].

In Figure 3 we reproduce the multiplets structure for $n = 11$ to $n = 14$. The $6snp\ ^3P_2$ line remains the dominant feature. With the increase of the principal

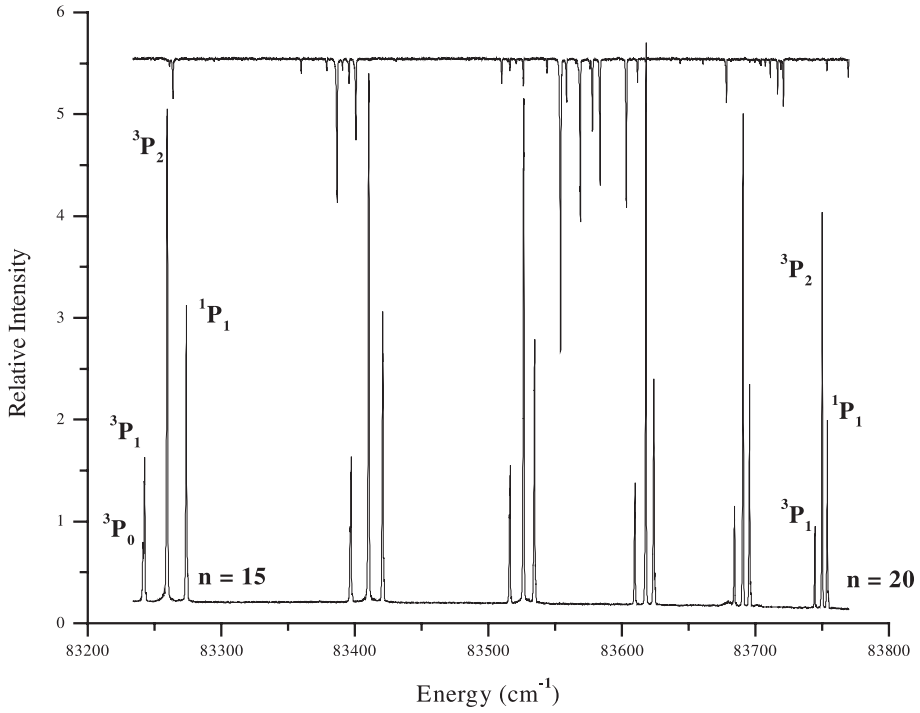

Fig. 4. The Rydberg series of mercury from $n = 15$ to $n = 20$ is shown. The top spectrum is the optogalvanic spectrum of neon hollow cathode lamp.

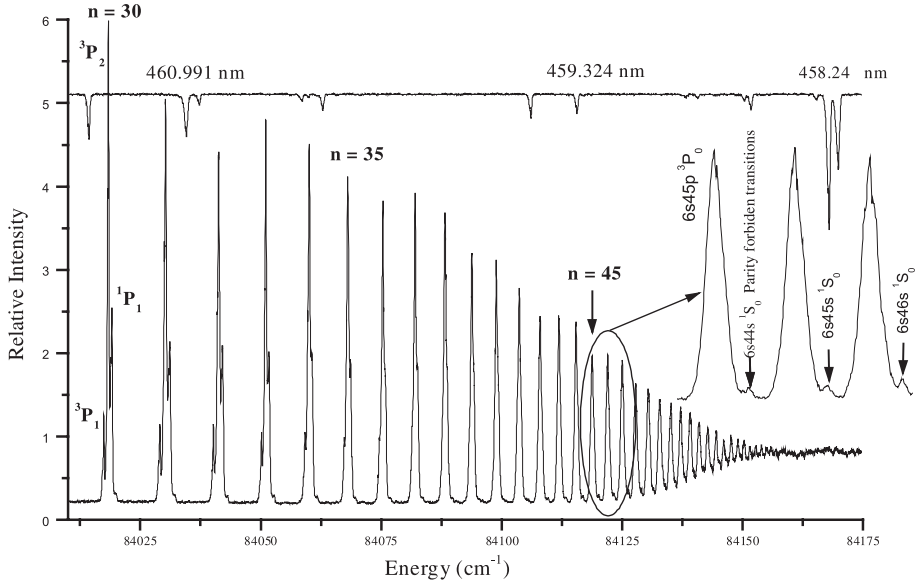

Fig. 5. The high Rydberg series of mercury from $n = 30$ to the series limit. The top spectrum is the optogalvanic spectrum of neon hollow cathode lamp, which acts as wavelength reference for the dye laser. The magnified view of a part of the mercury spectrum is also shown around $n = 45$ to make the parity forbidden transitions more prominent.

quantum number the separation between the multiplets decreases whereas, the trend of the relative intensities remains the same as observed for $6s10p$ configuration based levels shown in Figure 2.

In Figure 4 the higher members of the Rydberg series i.e. $n = 15{-}20$ are reproduced. The top spectrum is the optogalvanic spectrum of neon filled hollow cathode lamp. The $6snp\ ^3P_0$ and $^3P_1$ components have been resolved up to $n = 18$, afterwards they merge together. After $n = 18$ there remains only three components that are identified as $6snp\ ^3P_1$, $^3P_2$ and $^1P_1$ respectively. In the entire range of the observed spectrum the $6snp\ ^3P_2$ remains the dominant series.

Figure 5 shows the highly excited Rydberg levels covering $n = 30$ up to the series limit. The top spectrum shows the reference lines of neon that are used as wavelength standards. As mentioned earlier the dominating Rydberg series is $^3P_2$, that has been observed upto $n = 70$. The $6snp\ ^1P_1$ can be resolved from $^3P_2$ up to $n = 42$, whereas $^3P_1$ have been resolved up to $n = 41$. It is evident that the intensities of the Rydberg levels decrease in accordance to the n^{-3} scaling factor.

A close inspection of the spectrum presented in Figure 5 reveals some additional lines in between the members of the $6s6p\ ^3P_2$ series. These additional lines begin to emerge around $n = 40$. These lines are attributed to the

parity forbidden transitions that are induced due to collisions. As the Rydberg atom is excited to high n-values, it becomes more fragile due to its large size and consequently the buffer gas atoms may occupy the space between the core and the excited electron. The collisions imply a partial overlap of wave functions at higher n-values and hence ℓ-mixing takes place that results the emergence of parity forbidden transitions. The contribution of such collisions will depend upon the vapor density of the atoms, pressure of the buffer gas and the type of the buffer gas. The relative intensities of the collisionally induced forbidden transitions to that of the allowed transitions give a measure of the mixing coefficient [26]. The temperature of the discharge cell was about 340 K and the corresponding vapor density of the mercury atoms was $\approx 6\times10^{14}$ cm^{-3} whereas the Ne buffer gas was at 1 Torr. The relative intensities of the parity forbidden lines to that of the $6s45p\ ^3\mathrm{P}_2$ series is about 2%. However, more experimental work is needed, either by varying the buffer gas pressure or changing the buffer gas, to extract a meaningful value of the mixing coefficient.

The parity forbidden lines have been identified as $6sns\ ^1\mathrm{S}_0$ ($40 \leq n \leq 58$). The identification of the series is based on the effective quantum numbers that have been calculated from the known lower members of the series. In the NBS table [22] the $6sns\ ^1\mathrm{S}_0$ series are reported up to $n = 21$. The absolute energies of the Rydberg states are determined by adding the energy of the $6s7s\ ^3\mathrm{S}_1$ level at 62350.456 cm^{-1} [22] in to the laser excitation energies. The energies and quantum defects of all the observed lines are tabulated in Tables 1 and 2. We also noticed that the widths of the spectral lines do not increase as the principal quantum number increases, which shows that there is a minimal contribution of any electric field, a possible cause of line broadening. The energy difference between the highest observed level is 0.6 cm^{-1} that is three times more than the laser line width whereas, the last observed level lies only 25.2 cm^{-1} below the first ionization limit.

Since we have been able to observe the high Rydberg states up to $n = 70$, therefore an accurate value of the first ionization potential can be extracted using the Rydberg relation:

$$E_n = IP - \frac{Ry}{(n-\mu_\ell)^2}.$$

A least square fit to the experimental data yield the $IP = 84184.15 \pm 0.05$ cm^{-1} and the quantum defect as 4.105(2). This value of the IP is in excellent agreement with that reported by Baig et al. [17] 84184.15 ± 0.07 cm^{-1} based on the photo absorption measurements using synchrotron radiation as the back ground source of continuum. This value is also not far from the value quoted in the NBS table 84184.1 cm^{-1}. Tursunov et al. [14] also reported the highly excited states in mercury using three-step laser excitation technique from the ground state adopting the excitation path:

$$6s^2\ ^1\mathrm{S}_0 \rightarrow 6s6p\ ^3\mathrm{P}_1 \rightarrow 6s7s\ ^3\mathrm{S}_1 \rightarrow 6snp\ ^3\mathrm{P}_{0,1,2}.$$

The ionization potential was determined as 84185.0 cm^{-1}, which is 0.9 cm^{-1} higher than the value reported in the NBS tables [22]. Tursunov et al. [14] observed the splitting of the $6snp\ ^3\mathrm{P}_{0,1,2}$ states with $n \leq 31$ and beyond this n-value the signal peaks might get distorted. In the present experiment we have also detected the $6snp\ ^3\mathrm{P}_0$ series up to $n = 18$, $6snp\ ^3\mathrm{P}_1$ series up to $n = 41$, $6snp\ ^3\mathrm{P}_2$ series up to $n = 70$ and $6snp\ ^1\mathrm{P}_1$ series up to $n = 42$. The only available data that can be compared with our data is that of Tursunov et al. [14]. Unfortunately, their identification of the observed lines is not in accordance to the NBS table [22]. Tursunov et al. [14] designated the multiplets for each principal quantum number n as $6snp\ ^3\mathrm{P}_0$, $^3\mathrm{P}_1$ and $^3\mathrm{P}_2$ respectively in order of increasing energy. This misidentification might have been based on the adopted excitation path namely: $6s^2\ ^1\mathrm{S}_0 \rightarrow 6s6p\ ^3\mathrm{P}_1 \rightarrow 6s7s\ ^3\mathrm{S}_1 \rightarrow 6snp\ ^3\mathrm{P}_{0,1,2}$. However, the observed energies are closer to that of $6snp\ ^3\mathrm{P}_1$, $^3\mathrm{P}_2$ and $^1\mathrm{P}_1$ series tabulated in the NBS table [22] as well as to that of $6snp\ ^3\mathrm{P}_1$ and $^1\mathrm{P}_1$ series reported by Baig et al. [17]. In the present work, we have detected all the four Rydberg series namely: $6snp\ ^3\mathrm{P}_{0,1,2}$ and $6snp\ ^1\mathrm{P}_1$ which confirms the earlier conclusion that the data of Tursunov et al. [14] infact correspond to $6snp\ ^3\mathrm{P}_1$, $^3\mathrm{P}_2$ and $^1\mathrm{P}_1$ series. At low n-values our measurements are in good agreement with that compiled in the NBS table [22].

Using $IP = 84184.15$ cm^{-1} and quantum defects for the series: $^3\mathrm{P}_0 = 4.210(5)$, $^3\mathrm{P}_1 = 4.199(5)$, $^3\mathrm{P}_2 = 4.101(5)$ and $^1\mathrm{P}_1 = 4.020(5)$, the difference between the calculated and the observed energies do not exceed 0.1 cm^{-1}. This shows that there is no systematic shift between the observed and the calculated energies, which might exist due to Stark effects. The last observed level lies 25.2 cm^{-1} below the first ionization potential. This energy region can further be unveiled with a better resolution; however we must also take into account the Inglis-Teller relation which might suppress the appearance of the high Rydberg states. From the termination of the high Rydberg series, one can estimate of the net electric field present in the interaction region using the combined Inglis-Teller and Holtzmark field expression [27]

$$F(\mathrm{V/cm}) = \frac{1.23\times10^9}{n_m^5}$$

where, n_m is the principle quantum number whose intensity is equal to the background continuum signal and the units of the electric field F are volts/cm. The last member of the series has been detected up to $n = 70$ and the corresponding electric field turns out to be about 0.73 volts/cm. The linear Stark shift, using the hydrogenic approximation is given by [28]

$$\Delta E = 6.42\times10^{-5} n(n_2 - n_1)F.$$

Here n_1 and n_2 are the parabolic quantum numbers whose values are from 0 to $(n-1)$. The maximum value of the shift for $n = 50$ is 0.1 cm^{-1} and 0.22 cm^{-1} at $n = 70$ which is well within the quoted experimental uncertainty in the observed energies.

In conclusion, we have presented new data on the high Rydberg states of mercury using the laser optogalvanic

Table 1. Term energies and effective quantum numbers of the 6*snp* series in mercury.

n	$^3P_0$ (cm^{-1})	n^*	$^3P_1$ (cm^{-1})	n^*	$^3P_2$ (cm^{-1})	n^*	$^1P_1$ (cm^{-1})	n^*
10	80902.22	5.782	80916.55	5.795	81022.77	5.892	81153.59	6.017
11	81800.57	6.785	81807.98	6.796	81873.85	6.892	81942.46	6.997
12	82374.54	7.787	82378.52	7.796	82422.63	7.893	82464.10	7.987
13	82763.41	8.789	82765.78	8.796	82796.78	8.894	82823.98	8.982
14	83039.02	9.789	83040.56	9.796	83063.21	9.894	83082.07	9.979
15	83241.71	10.791	83242.59	10.796	83259.54	10.894	83273.35	10.976
16	83394.72	11.790	83395.46	11.796	83408.47	11.894	83418.72	11.974
17	83513.40	12.791	83513.87	12.795	83524.19	12.895	83532.13	12.973
18	83607.30	13.793	83607.48	13.795	83615.80	13.895	83622.02	13.972
19			83682.89	14.796	83689.54	14.895	83694.58	14.972
20			83744.37	15.796	83749.87	15.896	83753.93	15.971
21			83795.19	16.797	83799.89	16.899	83803.24	16.973
22			83837.63	17.796	83841.62	17.899	83844.47	17.974
23			83873.54	18.796	83876.96	18.900	83879.30	18.973
24			83904.15	19.797	83907.08	19.901	83909.10	19.974
25			83930.51	20.800	83932.97	20.902	83934.72	20.975
26			83953.22	21.799	83955.42	21.903	83956.97	21.978
27			83973.02	22.798	83974.96	22.903	83976.31	22.978
28			83990.46	23.803	83992.08	23.903	83993.25	23.976
29			84005.73	24.800	84007.21	24.904	84008.29	24.980
30			84019.35	25.805	84020.62	25.904	84021.58	25.981
31			84031.43	26.805	84032.59	26.908	84033.46	26.985
32			84042.18	27.802	84043.27	27.910	84044.04	27.986
33			84051.88	28.804	84052.85	28.910	84053.52	28.984
34			84060.63	29.806	84061.44	29.904	84062.04	29.978
35			84068.49	30.803	84069.26	30.905	84069.82	30.982
36			84075.70	31.810	84076.33	31.903	84076.85	31.980
37			84082.19	32.807	84082.79	32.904	84083.22	32.974
38			84088.19	33.816	84088.68	33.903	84089.10	33.978
39			84093.60	34.811	84094.07	34.902	84094.43	34.973
40			84098.60	35.816	84099.02	35.904	84099.42	35.989
41			84103.16	36.810	84103.59	36.908	84103.92	36.984
42					84107.78	37.906	84108.10	37.986
43					84111.66	38.909		
44					84115.23	39.904		
45					84118.56	40.903		
46					84121.65	41.901		
47					84124.51	42.897		
48					84127.20	43.897		
49					84129.73	44.905		
50					84132.11	45.920		
51					84134.28	46.907		
52					84136.34	47.907		
53					84138.27	48.906		
54					84140.08	49.901		
55					84141.80	50.904		
56					84143.42	51.908		
57					84144.93	52.896		
58					84146.37	53.895		
59					84147.75	54.907		
60					84149.04	55.902		
61					84150.26	56.908		
62					84151.42	57.904		
63					84152.52	58.902		
64					84153.56	59.894		
65					84154.57	60.908		
66					84155.51	61.897		
67					84156.41	62.896		
68					84157.27	63.894		
69					84158.10	64.904		
70					84158.88	65.905		

Table 2. Parity forbidden transitions $6sns\ ^1S_0$.

n	$^1S_0$ (cm^{-1})	n^*
40	84105.44	37.339
41	84109.51	38.343
42	84113.26	39.345
43	84116.76	40.353
44	84120.02	41.366
45	84122.97	42.352
46	84125.75	43.348
47	84128.36	44.350
48	84130.78	45.345
49	84133.09	46.359
50	84135.20	47.348
51	84137.22	48.356
52	84139.08	49.344
53	84140.84	50.336
54	84142.55	51.361
55	84144.09	52.338
56	84145.61	53.361
57	84147.03	54.372
58	84148.35	55.365

technique in conjunction with RF discharge cell. The full multiplicity of the $6snp$ configuration has been resolved. The strongest series $6snp\ ^3P_2$ has been extended up to $n = 70$ that yield an accurate value of the first ionization potential of mercury, in agreement to that presently accepted value. The collisionally induced parity forbidden transitions $6sns\ ^1S_0$ have also been observed near the series limit. It is also observed that the shifts in the levels, if present, are within our experimental errors.

References

1. J.E.M. Goldsmith, J.E. Lawler, Contemp. Phys. **22**, 235 (1981)
2. B. Barbieri, N. Beverini, A. Sasso, Rev. Mod. Phys. **62**, 603 (1990)
3. T.F. Gallagher, *Rydberg Atoms* (Cambridge Univ. Press, 1994)
4. J.P. Connerade, *Highly Excited Atoms* (Cambridge Univ. Press, 1998)
5. W. Demtroeder, *Laser Spectroscopy* (Springer Verlag, 1998)
6. P. van de Weijer, R.M.M. Cremers, Opt. Commun. **53**, 109 (1985)
7. P. van de Weijer, R.M.M. Cremers, J. Appl. Phys. **57**, 672 (1985)
8. J. Kramer, J. Appl. Phys. **64**, 1758 (1988)
9. W.H. Richardson, L. Maleki, E. Gamire, Phys. Rev. A **36**, 5713 (1987)
10. E.C. Benck, J.E. Lawler, J.T. Dakin, J. Opt. Soc. Am. B **6**, 11 (1989)
11. L. Sarger, E. Freysz, B. Couillaud, A. Ducasse, Opt. Commun. **61**, 26 (1987)
12. N. Bras, J.C. Jeannet, D. Perrin, J. Phys. B: At. Mol. Opt. Phys. **26**, 2289 (1993)
13. M.A. Baig, J. Phys. B: At. Mol. Phys. **16**, 1511 (1983)
14. A.T. Tursunov, N.B. Eshkobilov, A.T. Khalmanov, Opt. Spectr. **68**, 294 (1990)
15. A.K. Kasimov, A.T. Tursunov, O. Tukhlibaev, R.M. Ayupov, Opt. Spectr. **84**, 12 (1998)
16. C. Tai, F.W. Dalby, Can. J. Phys. **55**, 434 (1977)
17. M.A. Baig, R. Ali, S.A. Bhatti, J. Opt. Soc. Am. **14**, 731 (1997)
18. R.D. May, P.H. May, Rev. Sci. Instrum. **57**, 2242 (1986)
19. G.R. Harrison, *Wavelength Tables* (The M.I.T. Press, Cambridge, 1982)
20. A.A. Radzig, B.M. Smirnov, *Reference Data on Atoms, Molecules, and Ions* (Springer Verlag, Berlin, 1985)
21. P. Dyer, G.C. Baldwin, C. Kittrell, G. Dan, E. Abramson, Appl. Phys. Lett. **42**, 311 (1983)
22. C.E. Moore, *Atomic Energy Levels* (NSRDS-NBS 35, Washington, D.C., 1971), Vol. III
23. H.G. Kuhn, *Atomic Spectra* (Longman, London, 1971)
24. B. Edlen, *Handbook of Physics* (Springer, Berlin, 1984), Vol. 27, p. 81
25. W.R.S. Garton, J.P. Connerade, Astrophys. J. **155**, 667 (1969)
26. J. Zhang, K.T. Lu, J. Phys. B: At. Mol. Phys. **20**, 5065 (1987)
27. B.N. Ganguly, J. Appl. Phys. **60**, 571 (1986)
28. H.E. White, *Introduction to Atomic Spectra* (McGraw Hill, 1986)